Optimization of Pressure-Retarded Osmosis with Hollow-Fiber Membrane Modules by Numerical Simulation

Kishimoto, Michimasa ; Tanaka, Yasuhiro ; Yasukawa, Masahiro ; Goda, Shohei ; Higa, Mitsuru ; Matsuyama, Hideto

(Citation)
Industrial & Engineering Chemistry Research,58(16):6687-6695

(Issue Date)
2019-04-24

(Resource Type)
journal article

(Version)
Accepted Manuscript

Optimization of pressure-retarded osmosis with hollow-fiber membrane modules by numerical simulation

Michimasa Kishimoto[a], Yasuhiro Tanaka[a], Masahiro Yasukawa[b,c], Shohei Goda[d], Mitsuru Higa[b,c], and Hideto Matsuyama[a*]*

a) Center for Membrane and Film Technology, Department of Chemical Science and Engineering, Kobe University, 1-1 Rokkodaicho, Nada-ku, Kobe 657-8501, Japan
b) Division of Applied Chemistry, Graduate School of Sciences and Technology for Innovation, Yamaguchi University, 2-16-1, Tokiwadai, Ube, Yamaguchi 755-8611, Japan
c) Blue Energy center for SGE Technology (BEST), Yamaguchi University, 2-16-1, Tokiwadai, Ube, Yamaguchi 755-8611, Japan
d) Membrane Research and Development Center, Toyobo. Co. Ltd., 2-1-1 Katata, Otsu, Shiga 520-0292, Japan

Corresponding authors
Hideto Matsuyama, TEL: +81-78-803-6180, E-mail: matuyama@kobe-u.ac.jp
Michimasa Kishimoto, TEL: +81-75-381-3196, E-mail: mkishimoto@people.kobe-u.ac.jp

Abstract

We optimized the operating conditions for maximizing power production by the pressure-retarded osmosis (PRO) process using seawater as the draw solution and river (pure) water as the feed solution using a simulation algorithm developed in our previous work combined with the Complex optimization method. The calculated results showed that the maximum power production was 104 W/module, i.e., 18.7 kW/m^3, under the optimum conditions. The optimum hydraulic pressure applied to the draw solution was slightly higher than half the osmotic pressure difference between the draw solution and the feed solution, which was derived from the theoretical optimum pressure without concentration polarization and solute leakage. We also optimized the operating conditions of hypothetical modules that have improved membrane water permeability (2, 3, 4, and 5 times higher than the current membrane permeability coefficients). Although the power production increased with increasing water permeability, the relationship was not linear. The effects of internal and external polarization of the salt concentration and the solute permeability on the power production became significant with increasing membrane permeability.

Keywords:

Pressure-retarded osmosis; Optimized energy production; Cellulose triacetate membrane; Hollow-fiber membrane module; Friction-concentration polarization model

1. Introduction

Pressure-retarded osmosis (PRO) has been proposed for the production of electric power. PRO works by exploiting the osmotic pressure difference between the two solutions such as seawater (as the high-salinity solution) and river water (as the low-salinity solution) using a semipermeable membrane process in which water permeates through the membrane from the low-salinity solution to the pressurized high-salinity solution. Electric power is then generated by releasing the pressurized seawater through a hydro-turbine.[1–4]

There are several module types, such as hollow fiber (HF),[5] spiral,[6,7] and flat-plate types[8] for use in pilot-scale PRO membrane modules. Among them, the HF module has advantages of strong pressure resistance, comparatively large membrane area per unit volume, and the appropriate flow patterns in the module.[5, 9-12]

The PRO process using brine produced by reverse osmosis (RO) has been widely investigated.[13] This is because the higher osmotic pressure of a saline solution can produce significant electric power. In the present study, we tried to estimate the maximum power production with an HF membrane module using seawater rather than brine as the draw solution and river water without salt as the feed solution. The investigation was carried out with the aid of numerical simulation and optimization.

In ideal conditions, the theoretical water flux across a membrane, J_w, can be calculated.[14]

$$J_w = A(\Delta\pi - \Delta P) \tag{1}$$

where A is the water permeation coefficient of the membrane, $\Delta\pi$ is the osmotic pressure difference across the membrane, and ΔP is the hydrostatic pressure difference across the membrane. If $\Delta\pi$ and A are constant, the electric power production, E, generated by the PRO process is given by:[14, 15]

$$E = J_w A_{area} \Delta P = A A_{area} (\Delta\pi - \Delta P)\Delta P \tag{2}$$

where A_{area} is the membrane area. In ideal conditions, the maximum power production is given by:

$$E_{max} = A A_{area} \frac{\Delta\pi^2}{4} \tag{3}$$

Thus, the maximum power production is obtained when $\Delta P = \frac{\Delta\pi}{2}$. It should be noted that the real PRO process includes salt leakage and concentration polarization in the support layer of the semipermeable membrane (internal concentration polarization, ICP) and boundary layer on the membrane surface (external concentration polarization, ECP), which results in a deviation in $\Delta\pi$ from the the osmotic pressure difference between the bulk draw solution (DS) and the bulk feed solution (FS). Furthermore, the salt concentration can vary with location in the module because of the mixing of the permeate and

bulk solution. The pressure drop of the bulk flow inside the HF membrane also reduces power production. Therefore, we must examine the effects of the operating conditions on the available electric power to optimize the process.

Shibuya et al. proposed a simple integral calculation model, developed from the friction concentration polarization (FCP) model,[16-18] to explain and predict HF module performance under forward osmosis (FO) operation theoretically.[9] In our previous study, we modified the model to improve the accuracy of the calculations by combining PRO theory for water flux and salt leakage, and we experimentally and theoretically investigated the pilot-scale performance of two types of HF modules under a wide range of PRO operating conditions, and examined the distribution of the pressure, salt concentration, and permeation flux inside the modules.[12]

We have improved the modified model for the optimization of the PRO process in the present study. The optimization algorithm is based on the Complex method developed by Box et al.,[19-21] which was used to estimate the deviation in the HF module performance from the ideal performance given by Eq. (2) and ideal optimal operating conditions. We have investigated the hurdles that must be overcome for the commercialization of osmotic power production.

2. Computational algorithms for PRO process optimization

2.1. Simulation of the PRO process

In our previous work, a modified analytical model based on the friction-concentration polarization (FCP) model, which combines PRO theory with water flux and salt leakage, was proposed to estimate the PRO process performance when using an HF module.[12] The calculated results agreed well with the experimental data under a wide range of conditions.

Figure 1 presents a scheme of the HF module. This figure shows the hollow-fiber module, which includes the hollow fiber with an active layer and porous support layer. The draw solution and feed solution flow into the shell side and bore side, respectively, i.e., active layer facing the DS (AL-DS) mode.

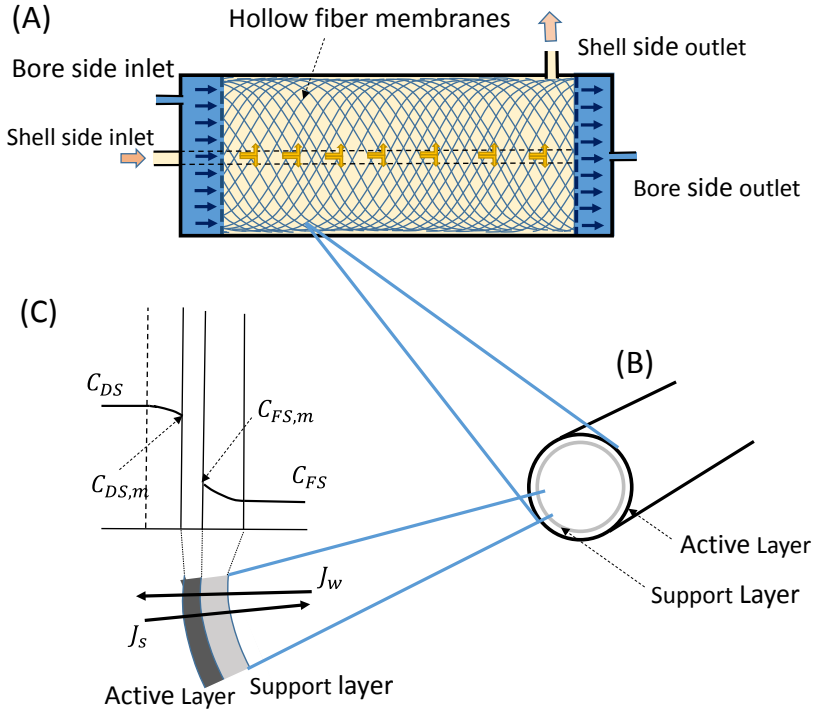

Fig. 1. Scheme of the modified model for the HF module. (A) PRO HF module with a cross-wound HF. (B) Cross-section of the HF with the outer active layer and the inner bore side support layer. (C) The salt concentration across the thin active layer.

We simulated the PRO process using hollow-fiber modules (1) and (2), which were kindly supplied by Toyobo Co., Ltd. The technical specifications of the modules and installed membranes are the same as those in our previous report[12] and are summarized in Tables 1 and 2.

Table 1

Specifications of the HF membrane modules.

	HF inner diameter d_{inner} [μm]	HF outer diameter d_{outer} [μm]	Module length [mm]	Number of fibers [-]	Effective membrane area [m^2]	Packing density [%]
Module (1)	85	175	682	220,000	70.5	54.2
Module (2)	117	189	682	165,600	65.6	43.2

Table 2
Intrinsic parameters of the HF membranes in the modules.

	Water permeability coefficient, A [L·m^{-2}·h^{-1}·bar^{-1}]	Salt permeability coefficient, B [L·m^{-2}·h^{-1}]	Structural parameter, S [μm]
Module (1)	0.27	0.035	1024
Module (2)	0.60	0.072	912

We used the model same as that in our previous work[12]. The osmotically driven water flux, J_w, was expressed by considering the membrane orientation and the internal and external concentration polarization effects as follows:[22]

$$J_w = A\left\{\frac{\pi_{DS,b}exp\left(-\frac{J_w}{k}\right)-\pi_{FS,b}exp\left(\frac{J_wS}{D_{diff}}\right)}{1+\frac{B}{J_w}\left[exp\left(\frac{J_wS}{D_{diff}}\right)-exp\left(-\frac{J_w}{k}\right)\right]}-\Delta P_{DS-FS}\right\} \quad (4)$$

where A, B, and S are the intrinsic parameters of the membrane, that is, the water permeability coefficient, solute permeability coefficient, and structural parameter, respectively. In addition, $\pi_{DS,b}$ [bar] and $\pi_{FS,b}$ [bar] are the osmotic pressures in the bulks of the more concentrated (DS) and less concentrated solutions (FS), respectively. ΔP_{DS-FS} [bar] denotes the hydraulic pressure difference between DS (shell side) and FS (bore side) of the HF membrane; and D_{diff} [μL·m^{-1}·h^{-1}] and k [L·m^{-2}·h^{-1}] are the diffusivity and mass transfer coefficient of the draw solute in the boundary layer on the membrane surface, respectively.

The fibers are wound spirally around a porous core tube. Therefore, the length of hollow fibers in the segment was calculated based on the precise analytical model proposed by Sekino,[16] and was used for the estimation of the effective membrane surface area in the segment.

In our previous study, we developed the following equation to estimate the net power production of the PRO system, where the efficiencies of the turbine and pressure exchanger were assumed to be 1:[12]

$$E = Q_{JW}P_{DS,out} - \left(Q_{DS,in}\left(P_{DS,in} - P_{DS,out}\right) + Q_{FS,in}P_{FS,in}\right) \quad (5)$$

Here, Q_{JW} is the volumetric flow rate of the permeated water.

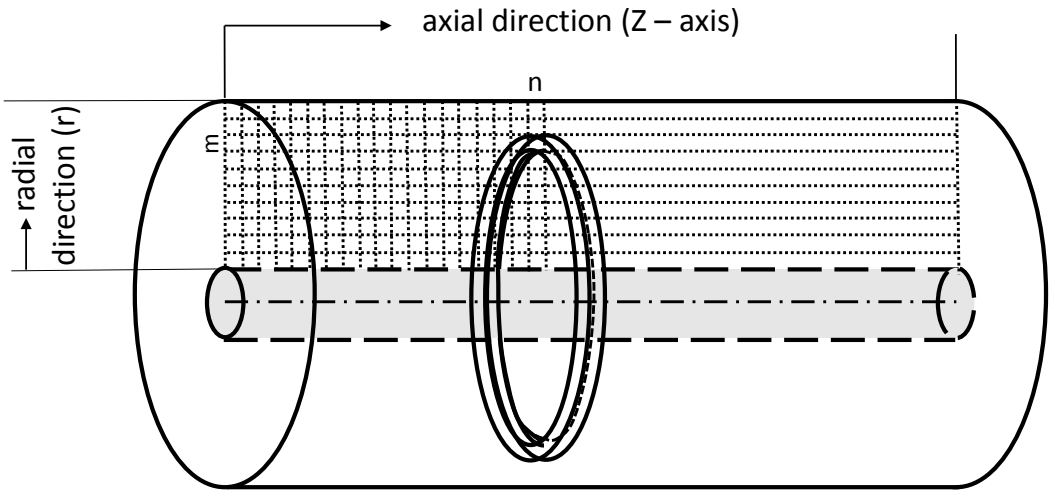

Fig. 2. Schematic view of the segmentation in the module for numerical simulation.

Figure 2 shows the segmentation in the module for the numerical simulation, which is carried out in cylindrical coordinates because the module is assumed to have cylindrical symmetry. The stepwise segmental (integral) calculation was performed in almost the same manner as in our previous work.[12] Because the permeate flux, J_W is found on both sides of Eq. (4), J_W was determined by least squares minimization between the estimated J_W value and the calculated result of the right-hand side of Eq. (4) based on golden-section search.[23] The integral calculation was carried out with 50,000 segmental cells (100 and 500 in the radial (r) and axial (z-axis) directions, respectively), and we confirmed that this number (50,000) was sufficient for accurate calculation in the present study.

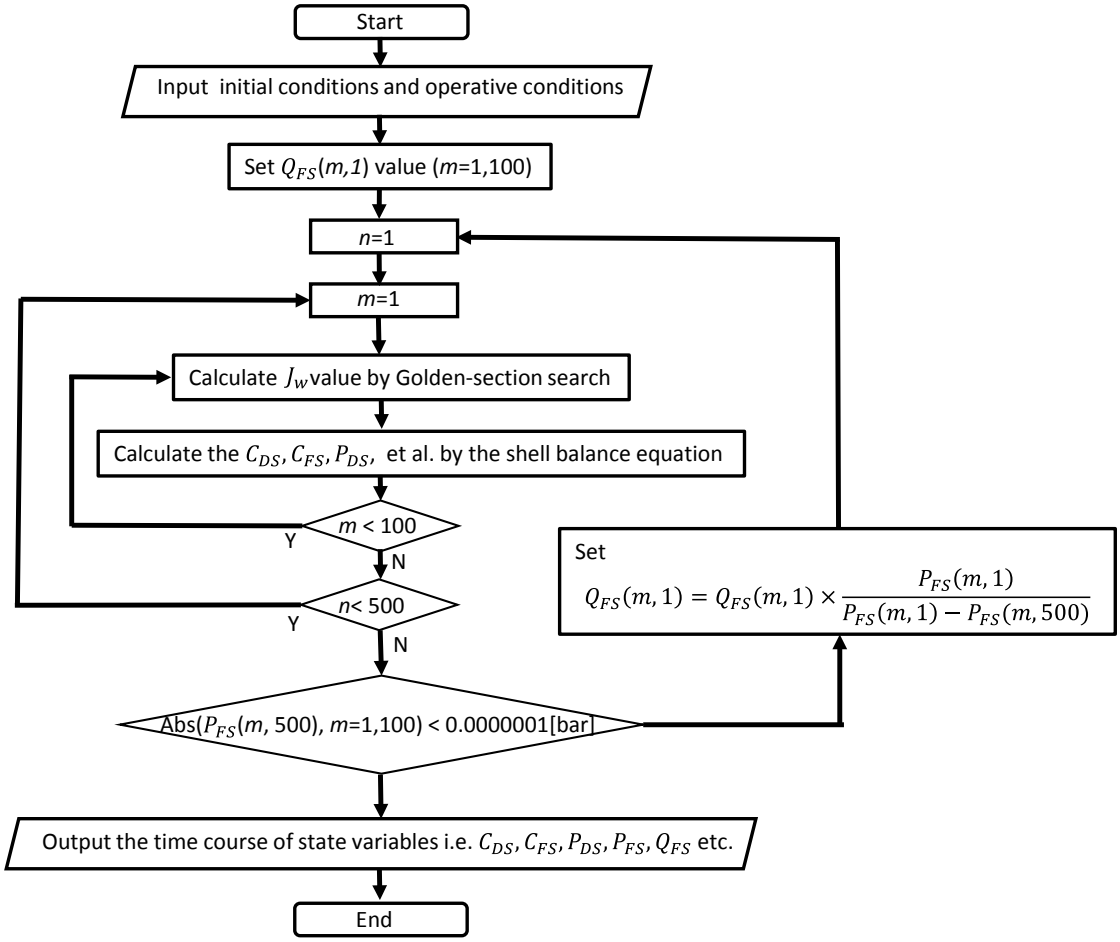

Fig. 3. Scheme for simulation of PRO HF module performance.

Figure 3 shows the scheme for the simulation of the PRO HF module performance. First, we input the initial conditions and operating conditions such as the inlet pressure of the draw solution ($P_{DS,in}$), inlet pressure of the feed solution ($P_{FS,in}$), and inlet volumetric flow rate of the draw solution ($Q_{DS,in}$). Then, we set the initial value of feed solution volumetric flow rate, Q_{FS}(m,1) with m = 1,100 at the module inlet, which was calculated using Eq. (6):

$$Q_{FS}(m,1) = \frac{\pi d_{inner}^4 P_{FS,in} \rho_{FS,in}}{128 \mu_{bore} L_{HF}} \quad (6)$$

where L_{HF} denotes the length of the HF.

For each segment, the J_W value was calculated using Eq. (4), and the other variables, e.g., C_{DS}, C_{FS}, and P_{DS} were calculated using shell balance equations. After these calculations, the end pressure of the bore side was checked at the module outlet. If the pressure error, that is, the deviation in the outlet pressure, $P_{FS}(m, 500)$, from 0 bar was larger than 0.0000001 bar, $Q(m, 1)$ was modified and returned to the initial step of the simulation. If the pressure deviation became smaller than the critical value, the simulation was finished. Using this algorithm, we can obtain information about the hydraulic pressure, salt concentration, and mass flow rate of each segment, and finally obtain the power

production defined by Eq. (5) under the given conditions for $P_{DS,in}$, $P_{FS,in}$, and $Q_{DS,in}$.

2.2. Optimization algorithm for the PRO process

The simulation procedure described above was combined with the Complex method[19-21] to optimize the operating conditions and to maximize the production of electric power. The objective is to maximize the power production, E, expressed by Eq. (5). The operating variables, which should be optimized by this program, are the inlet pressure of the draw solution ($P_{DS,in}$), inlet pressure of the feed solution ($P_{FS,in}$), and inlet volumetric flow rate of the draw solution ($Q_{DS,in}$). In the optimization, the initial values of these variables were generated randomly. The basic idea of the algorithm is to replace the worst point of minimum power production by a new point obtained by reflecting the worst point through the centroid of the remaining points in the complex as shown in Fig. 4. From the optimization results, the maximum power production and optimum operating conditions can be obtained.

However, it is possible that there are other optimum points. Therefore, we carried out simulations to estimate the power production for each point of the operating variables, as shown in Figs. 5 and 7, and we checked the unimodal shape of the power production plot around the maximum points relating to the operating variables.

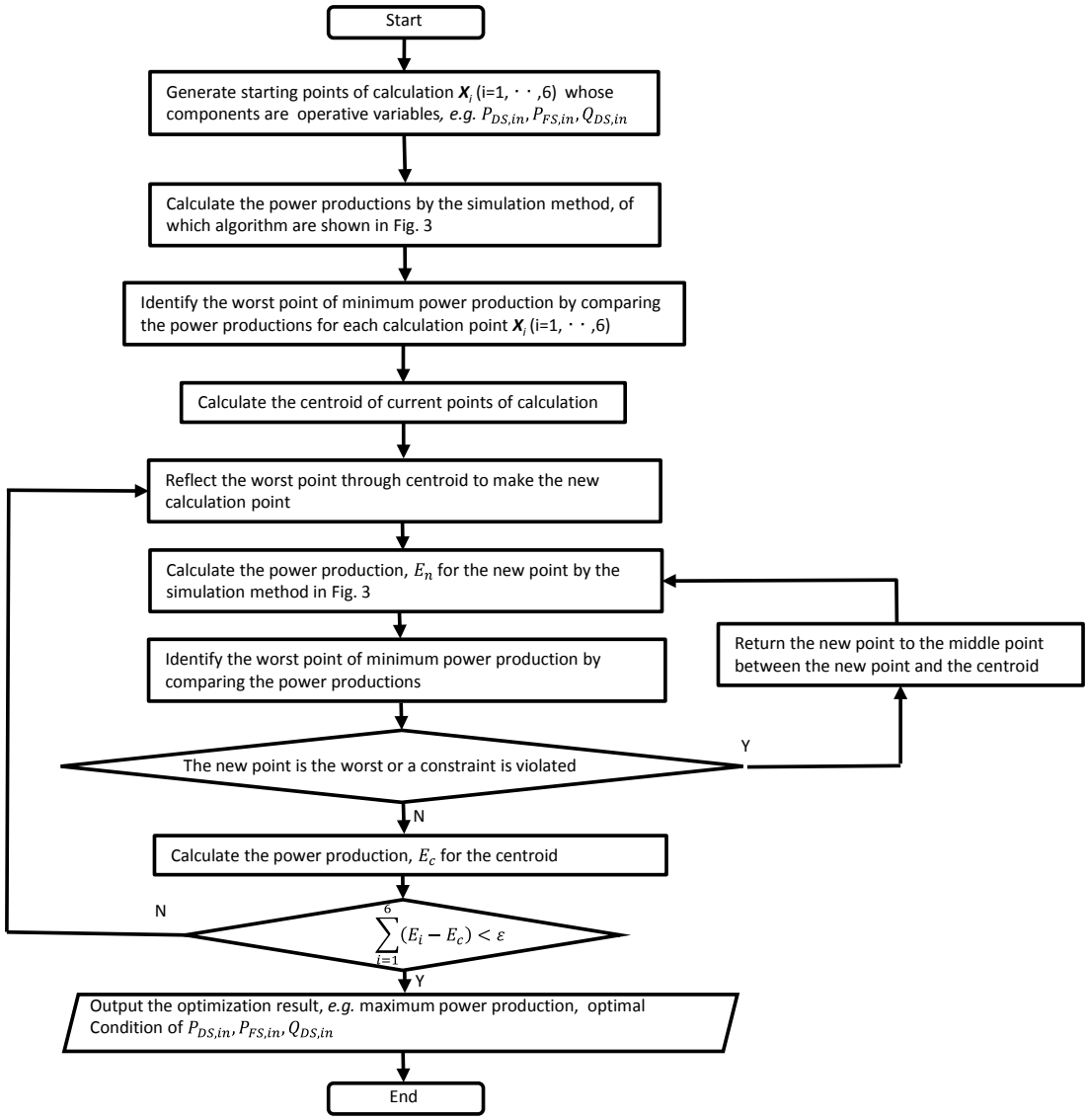

Fig. 4. Optimization algorithm for the PRO process with HF modules.

3. Results and Discussion

3.1. Optimum power-maximizing conditions for two hollow-fiber modules

Optimum conditions for maximizing the power production defined by Eq. (5) were calculated using seawater as a model draw solution and river water as a model feed solution. The draw solution and feed solution contain of 35 g/L (seawater level) and 0 g/L NaCl, respectively. The operating variables, which were optimized for maximum power production, are the pressure of the input draw solution, $P_{DS,in}$, the pressure of the input feed solution, $P_{FS,in}$, and the volumetric inlet flow rate of the draw solution, $Q_{DS,in}$.

Table 3
Optimal conditions for maximizing power production using seawater as a draw solution.

	$P_{DS,in}$ [MPa]	$P_{FS,in}$ [MPa]	$Q_{DS,in}$ [m^3/S]	*E/packed volume* [kW/m^3]
Module (1)	1.45	0.108	0.00099	13.8
Module (2)	1.00	0.146	0.00156	18.7

The optimal conditions for maximizing power production using module (1) are summarized in Table 3. The optimal $P_{DS,in}$ was 1.45 MPa and was slightly higher than half the osmotic pressure difference between the draw and feed solutions (1.37 MPa). The maximum power production per membrane packed volume using module (1) was 13.8 kW/m^3. The optimal conditions for maximizing the power production using module (2) are also summarized in Table 3. Because the membrane inside module (2) is soft and the upper limit of the applied pressure is 1.0 MPa for this module, the optimal pressure is equal to this upper limit pressure of 1.0 MPa. The maximum power production is 18.7 kW/m^3. This higher power production is attributable to the higher water permeability of the membrane inside module (2), as shown in Table 2.

We must confirm the unimodal shape of the power production plot with respect to the operational variables, i.e., $P_{DS,in}$, $P_{FS,in}$, and $Q_{DS,in}$, around the optimum conditions. Figure 5(A) shows the effects of $P_{DS,in}$ and $P_{FS,in}$ on the power production around the optimum condition in the case of module (1). The horizontal and vertical axes are the dimensionless parameters $\frac{P_{FS,in}}{P_{FS,in-opt}}$ and $\frac{P_{DS,in}}{P_{DS,in-opt}}$, respectively. $P_{FS,in-opt}$ and $P_{DS,in-opt}$ are the respective pressures under optimum conditions. Every point on the *z*-axis in this figure represents the power production at the$\left(\frac{P_{FS,in}}{P_{FS,in-opt}}, \frac{P_{DS,in}}{P_{DS,in-opt}}\right)$ coordinate, which was calculated using the simulation algorithm shown in Fig. 3. The effect of $P_{\text{DS-in}}$ on the power production is much larger than that of $P_{\text{FS-in}}$. From Eq.(5), the power production is directly affected by $P_{\text{DS,out}}$, and decreased sharply with the decrease of $P_{\text{DS,in}}$ under lower $P_{\text{DS,in}}$ than $P_{\text{DS,in-opt}}$. On the other hand, the osmotically driven water flux, J_w, which was strongly related to the power production, was significantly affected by $P_{\text{DS-FS}}$, and decreased sharply with the increase of $P_{\text{DS,in}}$ under higer $P_{\text{DS,in}}$ than $P_{\text{DS,in-opt}}$. Therefore we need to control the PDS-in precisely. On the other hand, the power production, *E*, sharply decreased with the decrease of $P_{\text{FS,in}}$ in the case of extreme low $P_{\text{FS,in}}$,. The decrease comes from the extreme low water permeate flux caused by the increase in the salt concentration in the feed solution, which comes from the extremely low velocity of the feed solution inside the hollow fiber.

Figure 5(B) also presents the effects of $P_{DS,in}$ and $Q_{DS,in}$ on the power production around the optimum condition. Power production is unimodal, as shown in both Figs. 5(A) and 5(B), and there is no other optimum point. $P_{DS,in}$ has a more significant effect than $P_{FS,in}$ and $Q_{DS,in}$. On the other hand, the effect of $Q_{DS,in}$ is very small in the range of $\frac{Q_{DS,in}}{Q_{DS,in-opt}} > 0.1$.

(A)

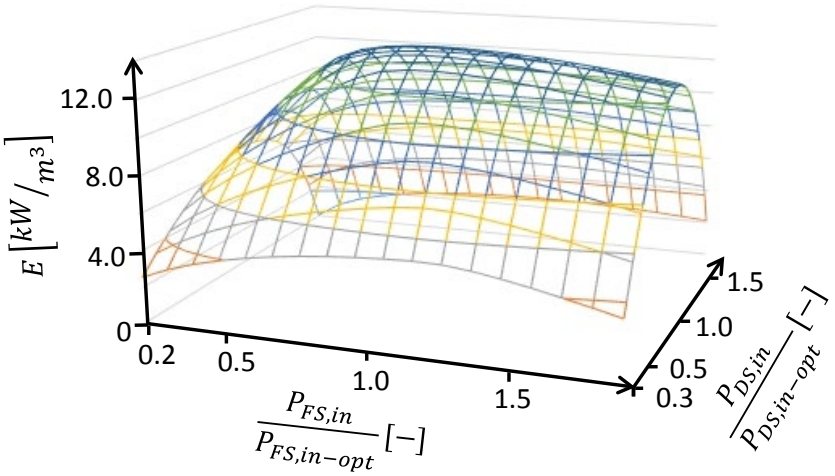

(B)

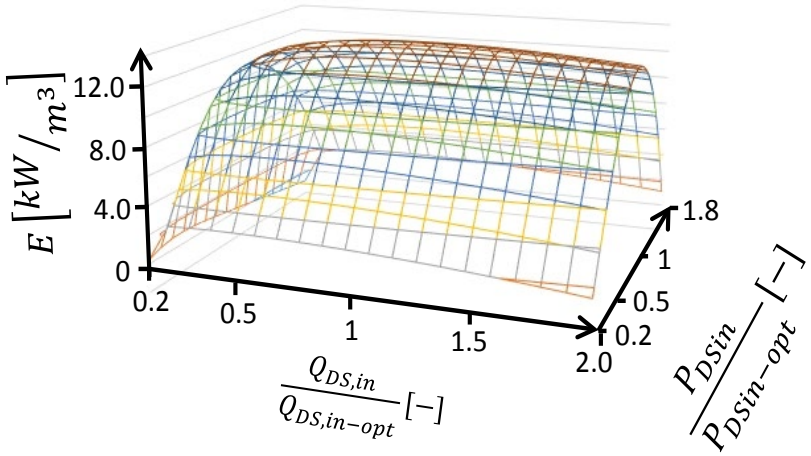

Fig. 5. Effects of $P_{DS,in}$, $P_{FS,in}$, and $Q_{DS,in}$ on hydraulic power production in the case of module (1): (A) Effects of $P_{DS,in}$ and $P_{FS,in}$ on power production, and (B) effects of $P_{DS,in}$ and $Q_{DS,in}$ on power production.

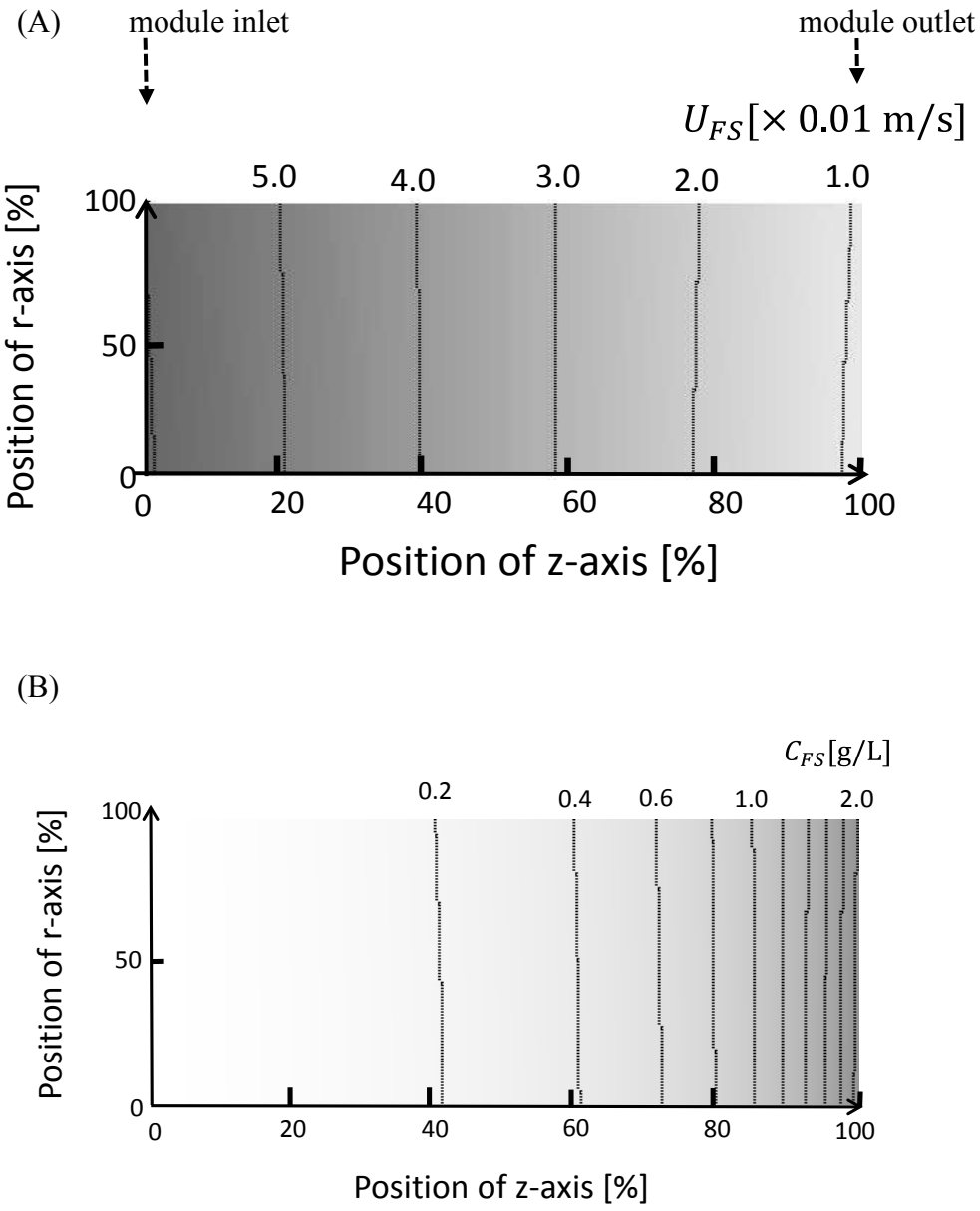

Fig. 6. Distribution of U_{FS} (A) and C_{FS} (B) within module (1) under optimum conditions.

Figure 6(A) shows the distribution of the linear velocity of the feed solution, u_{FS}, under optimum conditions. The linear velocity is low at the outlet of the hollow-fiber module. The optimal inlet pressure of the feed solution $P_{FS,in}$ should be set to a low level to avoid excess power loss for pumping the feed solution. However, we need to avoid an extremely low flow rate of the feed solution because of the increase in the salt concentration in the feed solution, C_{FS}, near the module outlet, as shown in Fig. 6(B). The increase in C_{FS} comes from the salt permeate through the membrane, and results in a reduction in the osmotic pressure difference between the inside and outside of the HF membrane. Therefore, precise control of the $P_{FS,in}$ is necessary.

(A)

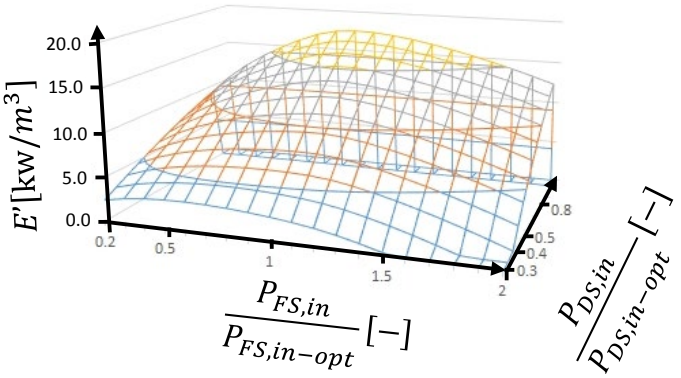

(B)

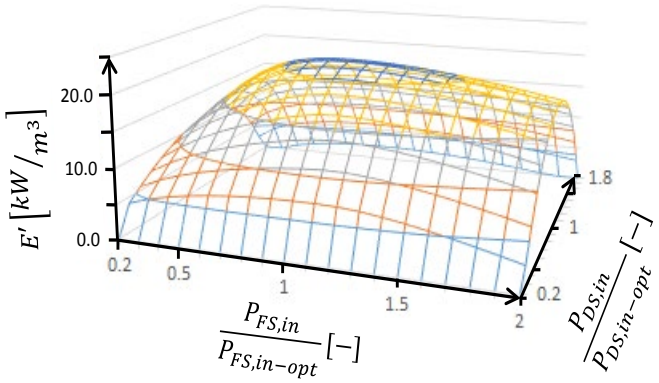

(C)

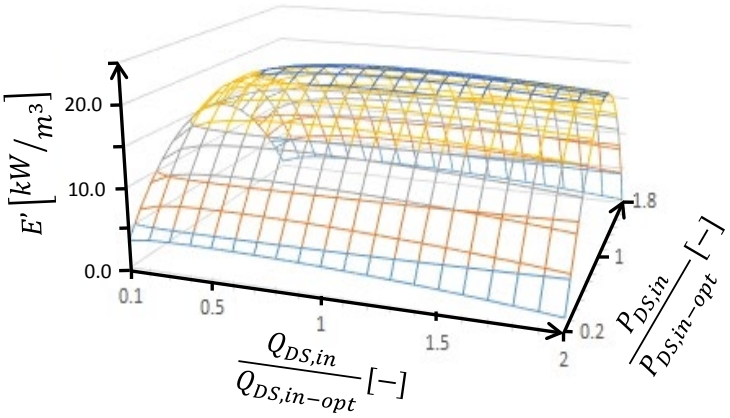

Fig. 7. Effects of $P_{DS,in}$, $P_{FS,in}$, and $Q_{DS,in}$ on hydraulic power production in the case of module (2). (A) effects of $P_{DS,in}$ and $P_{FS,in}$ on power production, (B) effects of $P_{DS,in}$ and $P_{FS,in}$ on power production without the upper limit of the pressure resistance around the optimum condition, and (C) effects of $P_{DS,in}$ and $Q_{DS,in}$ on power production without the upper limit of the pressure resistance around the optimum condition.

Figure 7(A) shows the effects of $P_{DS,in}$ and $P_{FS,in}$ on power production using module (2) around the optimum condition. As described above, the pressure resistance of the hollow fiber in module (2) is low (ca. 1.0 MPa) and, thus, $P_{DS,in-opt}$ was 1.0 MPa. This figure shows that the maximum power production was obtained at a $P_{DS,in}/P_{DS,in-opt}$ value of 1, that is, at the limited pressure. Thus, the pressure resistance of the module is very important for achieving high power production.

We also investigated the power production of a hypothetical module (2) that has no upper limit of the pressure resistance, but the other specifications are the same as those of model (2). Figure 7(B) shows the effects of $P_{DS,in}$ and $P_{FS,in}$ on power production using module (2) without an upper limit on the pressure resistance. Figure 7(C) shows the effects of $P_{DS,in}$ and $Q_{DS,in}$ using module (2) without an upper limit on the pressure resistance. From these calculated results, the power production schemes are unimodal, and there is no other optimum point. Thus, $P_{DS,in}$ is a much more sensitive variable than the other operational variables.

The optimum $Q_{DS,in}$ is small because this avoids excess pumping power losses, as shown in Table 3. However, the influence of $Q_{DS,in}$ is small compared with those of $P_{DS,in}$ and $P_{FS,in}$, as shown in Figs. 5(B) and 7(C). The inlet pressure of the feed solution, $P_{FS,in}$, should be set to a low level to prevent excess power loss for pumping the feed solution. In previous work, the distribution of water flux within the modules has been presented.[12] It was found that some areas inside module cannot be effectively utilized because of the low water permeation in these areas of the module. The feed solution should be supplied smoothly to all the module area by feeding pump. However, energy loss on pumping the feed solution through the very narrow space inside the thin hollow fiber must be avoided, which means the pressure drop is not negligible. Therefore, $P_{FS,in}$ should be optimized precisely. In the case of module (1), $P_{FS,in\text{-}opt}$ was determined to be 0.115 MPa as shown in Table 3, and the energy loss for pumping the feed solution is 1.56 kW/m^3, which is not negligible compared with the power production, 13.8 kW/m^3. $P_{FS,in\text{-}opt}$ of module (2) is 0.151 MPa, and the energy loss for pumping the feed solution is 2.18 kW/m^3, which also is not negligible compared with the power production, 18.7 kW/m^3.

3.2. Effect of the membrane water permeability

Figure 8 shows the effect of water permeability, A, on power production. The values of A were changed in the simulation, ignoring the real values, as shown in this figure. The power production under optimum conditions was estimated based on a combination of the simulation method and Complex method shown in Figs. 3 and 4. In the real modules, power production by module (2) is greater than that by module (1) because of the higher water permeability, as shown in Table 3. However, module (2) has a disadvantage of low pressure resistance, that is, we cannot operate module (2) at more than 10 bar. The increase in the power production of the module (2) decreased in the high A region because of pressure limitations, and power production by module (1) becomes larger than that of

module (2) with the same A. Even if the pressure resistance is improved and there is no pressure limitation, the salt leakage shown in Table 2 affects power production in module (2), which leads to still lower power production than that of module (1) with the same A.

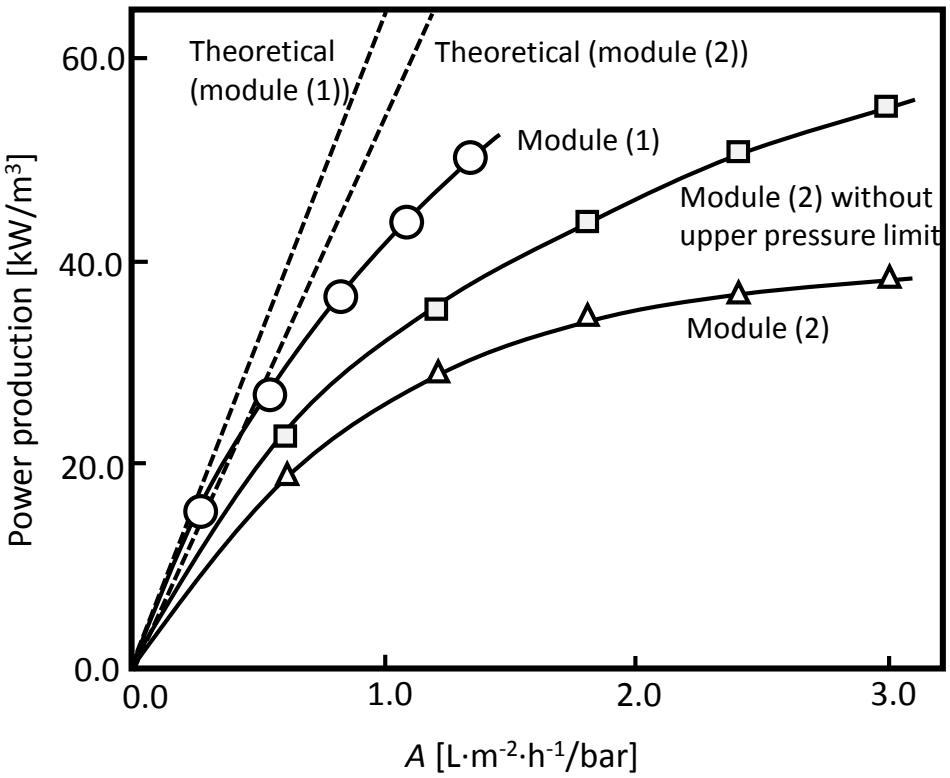

Fig. 8. Optimization of the maximum power production with the increase in water permeability coefficient, A, of module (1), module (2), and module (2) without an upper pressure limit.

The broken lines marked theoretical (module (1)) and theoretical (module (2)) in Fig. 8 represent the theoretical maximum power production calculated using Eq. (3) assuming ideal conditions, i.e., no salt leakage, unlimited pressure resistance, and no concentration polarization. Comparing between Eq. (1) and Eq. (4), it should be noticed that the deviation of J_W value, which calculated by Eq. (4), from J_W value in ideal condition, which calculated by Eq. (1), increases with the increase of J_W value. Therefore, the larger deviation of the power production by the actual module (2) from the theoretical power production compared with that by module (1) came from the larger J_W value of the module (2). We investigated these effects quantitatively in the case of module (2). If the pressure resistance was sufficiently high for optimum operation, the power production would increase to 15.6%. In the case of no upper limit of pressure resistance, the improvement by introducing the ideal conditions was estimated as follows. If the B value, which represents salt leakage through the membrane, is zero, power production can increase to 15.2%. If the mass transfer coefficient in the boundary layer on the active layer of the membrane increases by 100 times, that is, the concentration

polarization in the layer (ECP) is negligible, the power production can increase to 8.6%. If salt transfer by diffusion in the support layer of the membrane is very large, that is, the concentration polarization in the support layer of the membrane (ICP) is negligible, the power production can increase to 10.2%. In extreme conditions (i.e., A is 5 times the real value), the increase in power production achieved by removing the barriers, i.e., the upper limit of pressure resistance, the salt leakage, ECP, and ICP, were calculated to be 45.5%, 42.2%, 16.3%, and 22.5%, respectively. Thus, these additional factors, as well as A, must be addressed to increase power production by improving the membrane and module structures.

Figure 9 presents the optimum inlet pressure, $P_{DS,in}$, of the draw solution for maximum power production. In module (1), $P_{DS,in}$ is higher than the theoretical value of $\Delta\pi/2$ arising from salt leakage and concentration polarization. This deviation from the theoretical value increases with increasing A because the effects of salt leakage and ICP become more significant at high J_w. The optimum pressure of module (2) is lower than $\Delta\pi/2$ and the same as the pressure resistance (1.0 MPa). In the calculations involving module (2) without an upper pressure limit, $P_{DS,in}$ was also higher than $\Delta\pi/2$ and increased with increasing A.

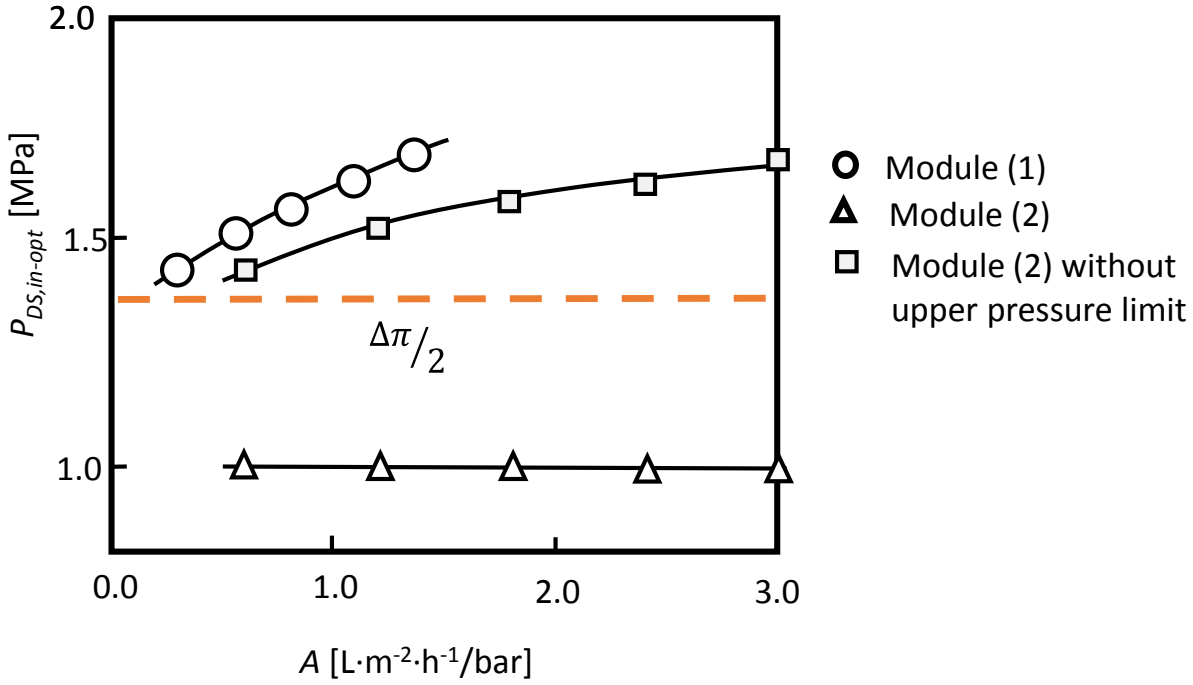

Fig. 9. Effect of A on $P_{DS,in-opt}$ for maximum power production.

4. Conclusion

The performance of the PRO process using two types of four-inch HF modules was investigated by numerical simulation. The calculation results showed that the power production was 13.8 kW/m^3 for module (1) and 18.7 kW/m^3 for module (2) under optimum conditions. The optimum

pressure of the draw solution is slightly higher than half the osmotic pressure difference between the draw solution and feed solution, which is the theoretical optimum pressure for maximizing electric power production. From the calculated results of the distribution of the flow rate of the feed solution in HF, it was noticed that the optimum flow rate of feed solution must be precisely regulated to avoid energy loss for the pumping feed solution and to supply the feed solution to every area of the module. The effect of the water permeability (A) of the membrane on the power production was calculated. Although increasing A improved power production, the power production became saturated at high A because of salt leakage and concentration polarization. In addition to the enhancement of A value, these factors must be considered to increase power production.

In the present study, we assumed that the energy recovery efficiency from the high-pressure output draw solution is 100%. However, if the efficiency is lower, the energy loss might become non-negligible. Furthermore, we must consider the effects of HF membrane fouling, that is, if the draw solution or feed water contained the organic, inorganic and microbial foulants, a fouling problem would occur, and the permeate flux in the module would decline significantly. [24-30] The optimization of PRO process considering with the fouling phenomena on the surface of membrane should be carried out for the practical use in future, even though the modeling of the fouling phenomena could not be carried out easily.

Nomenclature

A	water permeability coefficient [$L \cdot m^{-2} \cdot h^{-1} \cdot bar^{-1}$]
A_{area}	effective membrane area [m^2]
B	solute permeability coefficient [$L \cdot m^{-2} \cdot h^{-1}$]
C	concentration [g/L]
D	inner diameter of shell [m]
d	hollow-fiber diameter [m]
D_{diff}	mutual diffusion coefficient [$\mu L \cdot m^{-2} \cdot h^{-1}$]
E	maximum power production [W]
E'	maximum power production per membrane packed volume [W/m^3]
F_N	number of fibers [-]
J_s	solute flux [$mol \cdot m^{-2} \cdot h^{-1}$]
J_w	water flux [$L \cdot m^{-2} \cdot h^{-1}$]
k	mass transfer coefficient [$L \cdot m^{-2} \cdot h^{-1}$]
L	length [m]
P	hydrostatic pressure [Pa]
$\Delta P_{DS\text{-}FS}$	hydrostatic pressure difference between DS and FS [bar]
Q	volumetric flow rate [L/h]
R	gas constant [$bar \cdot L \cdot mol^{-1} \cdot K^{-1}$]

r	coordinate in the radial direction of the module [m]
Re	Reynolds number [-]
S	structure parameter of the support layer [μm]
Sc	Schmidt number [-]
Sh	Sherwood number [-]
T	temperature [K]
u	linear velocity of solution [$m \cdot s^{-1}$]
z	coordinate in the axial direction of the module [m]

Greek letters

ε	porosity of the support layer [-]
μ	viscosity [Pa·s]
v	van't Hoff factor [-]
π	osmotic pressure [Pa]
ρ	density [$kg \cdot m^{-3}$]
τ	tortuosity of the support layer [-]

Subscripts

b	at bulk
bore	inner bore-side of HF
DS	draw solution side
FS	feed solution side
HF	hollow-fiber membrane
in	at inlet
inner	inner value
JW	permeated water
m	at membrane active layer surface
max	maximum
opt	optimum
out	at outlet
outer	outer

References

(1) Thorsen, T.; Holt, T. The potential for power production from salinity gradients by pressure retarded osmosis. J. Membr. Sci. **2009**, *335* (1-2), 103.

(2) Achilli, A.; Cath, T. Y.; Childress, T. E. Power generation with pressure retarded osmosis: An

experimental and theoretical investigation. J. Membr. Sci. **2009**, *343* (1-2), 42.

(3) Loeb, S. Large-scale power production by pressure-retarded osmosis using river water and sea water passing through spiral modules, Desalination **2005**, *143* (2), 115.

(4) Touati, K.; Tadel, F.; Kim, J. H.; Alvarez-Silva, O., Pressure retarded osmosis: renewable energy generation and recovery, Academic Press 2017.

(5) Higa, M.; Shigefuji, D.; Shibuya, N.; Izumikawa, S.; Ikebe, Y.; Yasukawa, M.; Endo, N.; Tanioka, A. Experimental study of a hollow fiber membrane module in pressure-retarded osmosis: module performance comparison with volumetric-based power outputs, Desalination **2017**, *420*, 45.

(6) Xu, Y.; Peng, X.; Tang, C. Y.; Fu, O. S.; Nie, S. Effect of draw solution concentration and operating conditions on forward osmosis and pressure retarded osmosis performance in a spiral wound module, J. Membr. Sci. **2010**, *348* (1-2), 298.

(7) Kim, Y.C.; Kim, Y.; Oh, D.; Lee, K. H. Experimental investigation of a spiral-wound pressure-retarded osmosis membrane module for osmotic power generation, Environ. Sci. Technol. **2013**, *47* (6), 2966.

(8) Desormeaux, E. Blue tech webinar series: A focus on pressure retarded osmosis, (March 20, 2014).

(9) Shibuya, M; Yasukawa, M.; Goda, S.; Sakurai, H.; Takahashi, T.; Higa, M.; Matsuyama, H. Experimental and theoretical study of a forward osmosis hollow fiber membrane module with a cross-wound configuration, J. Membr. Sci. **2016**, *504*, 10.

(10) Shibuya, M.; Yasukawa, M.; Takahashi, T.; Miyoshi, T.; Higa, M.; Matsuyama, H. Effect of cellulose triacetate forward osmosis hollow fiber membrane. *Desalination* **2015**, *362*, 34.

(11) Shibuya, M.; Yasukawa, M.; Takahashi, T.; Miyoshi, T.; Higa, M.; Matsuyama, H. Effects of operating conditions and membrane structures on the performance of hollow fiber forward osmosis membranes in pressure assisted osmosis. Desalination **2015**, *365*, 381.

(12) Tanaka, Y.; Yasukawa, M.; Goda, S.; Sakurai, H.; Shibuya, M.; Takahashi, T.; Kishimoto, M.; Higa, M.; Matsuyama, H. Experimental and simulation studies of two types of 5-inch scale hollow fiber membrane modules for pressure-retarded osmosis, Desalination **2018**, *447*, 133.

(13) Kurihara, M.; Hanakawa, M. Mega-ton water system: Japanese national research and development project on seawater desalination and wastewater reclamation, Desalination **2013**, *308*, 131.

(14) Lee, K. L.; Baker, R. W.; Lonsdale, H. K. Membranes for power generation by pressure-retarded osmosis, J. Membr. Sci. **1981**, *8* (2), 141.

(15) Li, M. Analysis and optimization of pressure retarded osmosis for power generation, AIChE J. **2015**, *61* (4), 1233.

(16) Sekino, M. Precise analytical model of hollow fiber reverse osmosis modules, J. Membr. Sci. **1993**, *85*, 241.

(17) Sekino, M. Study of an analytical model for hollow fiber reverse osmosis module systems,

Desalination **1995**, *100* (1-3), 85.
(18) Kumano, A.; Matsuyama, H. Analysis of hollow fiber reverse osmosis membrane module of axial flow type, J. Appl. Polym. Sci. **2012**, *123* (1), 463.
(19) Box, M. J. A new method of constrained optimization and a comparison with other methods, Comput. J. **1965**, *8* (1), 42.
(20) Spendley, W.; Hext, G. R.; Himsworth, F. R. Sequential application of simplex designs in optimisation and evolutionary operation, Technimetrics **1962**, *4* (4), 441.
(21) Nelder, J. A.; Mead, R.; A simplex method for function minimization, Comput. J. **1965**, *7* (4), 308.
(22) Yip, N. Y.; Tiraferri, A.; Phillip, W. A.; Schiffman, J. D.; Hoover, L. A.; Kim, Y. C.; Elimelech, M.; Thin-film composite pressure retarded osmosis membranes for sustainable power generation from salinity gradients, Environ. Sci. & Technol. **2011**, *45* (10), 4360.
(23) Kiefer, J. Sequential minimax search for a maximum, Pro. Am. Math. Soc. **1953**, *4* (3), 502.
(24) Zhang, M.; Hou, D.; She, Q.; Tang, C. Y. Gypsum scaling in pressure retarded osmosis: experiments, mechanisms and implications. *Water Res.* **2014**, *48*, 387.
(25) She, Q.; Wong, Y. K. W.; Zhao, S.; Tang, C. Y. Organic fouling in pressure retarded osmosis: experiments, mechanisms and implications. *J. Membr. Sci.* **2013**, *428*, 181.
(26) Chen, S. C.; Fu, X. Z.; Chung, T. S. Fouling behaviors of polybenz-imidazole (PBI)-1146 polyhedral oligomeric silsesquioxane (POSS)/polyacrylonitrile (PAN) hollow fiber membranes for engineering osmosis processes. *Desalination* **2014**, *335*, 17.
(27) Chen, S.C.; Wan, C. F.; Chung, T. S. Enhanced fouling by inorganic and organic foulants on pressure retarded osmosis (PRO) hollow fiber membranes under high pressures. *J. Membr. Sci*. **2015**, 479, 190.
(28) Thelin, W. R.; Sivertsen, E.; Holt, T.; Brekke, G. Natural organic matter fouling in pressure retarded osmosis. *J. Membr. Sci.* **2013**, 438, 46.
(29) Yip, N. Y.; Elimelech, M. Influence of natural organic matter fouling and osmotic backwash on pressure retarded osmosis energy production from natural salinity gradients. Environ. Sci. Technol. **2013,** *47*, 12607.
(30) Bar-Zeev, E.; Perreault, F.; Straub, A. P.; Elimelech, M. Impaired performance of pressure-retarded osmosis due to irreversible biofouling. *Environ. Sci. Technol.* **2015**, *49*, 13050.

For Table of Contents Only